Nanoscale

COMMUNICATION

Cite this: *Nanoscale*, 2019, **11**, 878

Received 19th October 2018,
Accepted 17th December 2018

DOI: 10.1039/c8nr08477g

rsc.li/nanoscale

Synthesis and characterization of a single-layer conjugated metal–organic structure featuring a non-trivial topological gap†

Zi'Ang Gao,[a] Chia-Hsiu Hsu,[b] Jing Liu,[a] Feng-Chuan Chuang,[c] Ran Zhang,[a] Bowen Xia,[a,b] Hu Xu,[b] Li Huang,*[b] Qiao Jin,[d] Pei Nian Liu *[d] and Nian Lin *[a]

We employ an on-surface assembly protocol to synthesize a single layer of a two-dimensional conjugated network ($Ni_3(HITP)_2$) on a Au(111) surface. The electronic coupling between the π orbital of the diimine ligand and the d orbital of the metal ion renders efficient π-conjugation. Density-functional theory calculations provide evidence of a non-trivial topological gap in the surface-adsorbed single layer. This work demonstrates that single-layer 2D metal–organic frameworks adsorbed on surfaces are a new class of 2D materials that host quantum phases.

Metal–organic frameworks (MOFs) are a class of porous materials composed of metal centers linked by organic ligands through coordination bonds.[1,2] Two-dimensional (2D) MOFs have attracted intensive attention recently in light of the rapidly emerging field of 2D materials.[3,4] In particular, some 2D-MOFs with a π-conjugated backbone have been demonstrated theoretically to exhibit non-trivial topological band structures that are associated with quantum phases.[5–7] In 2013, Liu *et al.* proposed that 2D-MOFs incorporating a hexagonal lattice of heavy atoms of Pb or Bi are quantum spin Hall (QSH) insulators.[5] A QSH insulator is a nonmagnetic insulator which harbors gapless edge states. These edge states lead to two spin-polarized currents propagating in opposite directions.[7] Later, it was proposed that replacing Pb by Mn or In in the same structure leads to the quantum anomalous Hall (QAH) effect.[8] Thereafter, various π-conjugated 2D-MOFs that comprise a Kagome lattice of metal atoms were predicted to host the quantum phases.[9–18]

In the last few years, there have been many efforts to synthesize π-conjugated 2D-MOFs.[19–31] However, the predicted quantum phase has not been observed. One of the major problems is that all these synthesized 2D-MOFs are in a thin film form but not in a single-layer form. For example, a single layer of $Ni_3(HITP)_2$ (HITP: 2,3,6,7,10,11-hexaiminotriphenylene) was predicted to host the QSH effect.[12] The synthesized films contain staked multiple $Ni_3(HITP)_2$ layers, which display a conductivity of 40 S cm^{-1},[22,31] but not QSH effects. This failure is not surprising because the quantum effects are very likely quenched by the inter-layer interactions in the multi-layer samples. In this regard, the synthesis of a single layer of these predicted 2D-MOFs is highly desirable.

In this work, we synthesize single-layer $Ni_3(HITP)_2$ on a Au(111) substrate using on-surface coordination self-assembly.[32] We resolved its structure at sub-molecular resolution using scanning tunneling microscopy (STM). The density-functional theory (DFT) calculations show that upon adsorption on Au(111), the single-layer $Ni_3(HITP)_2$ interacts weakly with the substrate and retains its planar structure. Interestingly, the non-trivial topological gap of the free-standing layer is preserved in the surface-adsorbed layer. These results demonstrate that on-surface self-assembly is a viable route to realize 2D-MOFs exhibiting exotic quantum phases.

2,3,6,7,10,11-Hexaaminotriphenylene (HATP, inset in Fig. 1a) was sublimed using an organic-beam evaporator and deposited on a clean single crystal Au(111) surface which was held at room temperature. The sample was characterized using scanning tunneling microscopy at room temperature. Only fuzzy features were observed, indicating that the HATP molecules were highly mobile on the surface at room temperature. After depositing Ni onto the sample and annealing the sample to 100 °C, a hexagonal network structure was observed. Further annealing the sample to 250 °C resulted in larger network domains, as shown in Fig. 1a. There exists two different lattice orientations with angles of ±6.5° mirrored with

[a]*Department of Physics, The Hong Kong University of Science and Technology, Hong Kong SAR, China. E-mail: phnlin@ust.hk*
[b]*Department of Physics, Southern University of Science and Technology, Shenzhen, Guangdong 518055, China. E-mail: huangl@sustc.edu.cn*
[c]*Department of Physics, National Sun Yat-Sen University, Kaohsiung 804, Taiwan*
[d]*Shanghai Key Laboratory of Functional Materials Chemistry and School of Chemistry & Molecular Engineering, East China University of Science and Technology, Meilong Road 130, Shanghai 200237, China. E-mail: liupn@ecust.edu.cn*

†Electronic supplementary information (ESI) available: Methods. See DOI: 10.1039/c8nr08477g

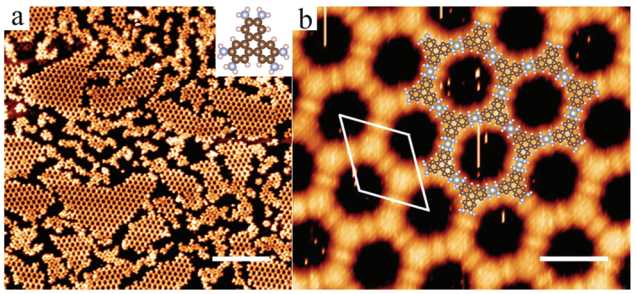

Fig. 1 Single-layer $Ni_3(HITP)_2$ network self-assembled on Au(111). (a) An overview STM image (inset: a molecular model of the HATP molecule, C: brown, N: blue, H: pink). Scale bar: 20 nm. (b) A high-resolution STM image overlaid with a molecular model (Ni: large blue balls). Scale bar: 2 nm.

respect to the [01−1] direction of the Au(111) substrate. Further enlarging the domain size was not successful, presumably because the diimine–Ni bonds are strong, thus favouring the growth of multiple smaller domains than a big single domain.

Because the network structure emerged after adding Ni, we conclude that this structure is a Ni-coordinated metal–organic framework formed by 2,3,6,7,10,11-hexaiminotriphenylene (HITP) after deprotonation of the amino groups of the HATP. Fig. 1b shows a high-resolution STM image. The hexagonal-shaped objects are assigned as HITP molecules according to their size and shape, and the oval-shaped objects are assigned as Ni atoms. Each HITP molecule links head-to-head, being bridged by a Ni atom, with three neighboring HITP molecules. The diamond shaped unit cell in Fig. 1b has a lattice constant of 2.17 ± 0.02 nm. We propose a model, which is overlaid in Fig. 1b, for this structure. In this model, four N atoms coordinate to a Ni atom in a 4-fold configuration. The 2D framework of $Ni_3(HITP)_2$ comprises a Kagome lattice of Ni atoms. This structure is almost identical to the $Ni_3(HITP)_2$ 2D-MOF (the unit cell size is 21.75 Å) in the multi-layer thin films synthesized by Sheberla *et al.*[22]

Zhao *et al.* studied the electronic properties (*i.e.*, Z_2 invariant, topological edge states, doping effect, and spin Hall conductance) of a free-standing $Ni_3(HITP)_2$ monolayer theoretically.[12] They found that this structure exhibits QSH effects and interesting Z_2 metallic states in different electron-doped regions. Here we used the DFT method to study the electronic properties of the single-layer $Ni_3(HITP)_2$ adsorbed on a Au(111) substrate. Fig. 2a shows the optimized atomic structure of the $Ni_3(HITP)_2$ network adsorbed on a Au(111)-$\sqrt{57} \times \sqrt{57}$ substrate composed of three layers of Au. The angle between the unit cell of the $Ni_3(HITP)_2$ network and the Au(111)-1 × 1 [01−1] direction is 6.587°, agreeing excellently with the experimentally observed domain orientations. The lattice constant is 21.89 Å, which is the same as the lattice constant of the free-standing single layer. The N–Ni distance is 1.840 Å. The side view (bottom panel of Fig. 2a) shows that the monolayer is a planar network. The Ni atoms are 3.460 Å above the Au substrate, implying that the monolayer interacts weakly with the Au substrate, as confirmed by a relatively small adsorption energy of 1.028 eV per unit cell. The right panel of Fig. 2c shows a simulated STM image which reproduces well the experimental data (left panel).

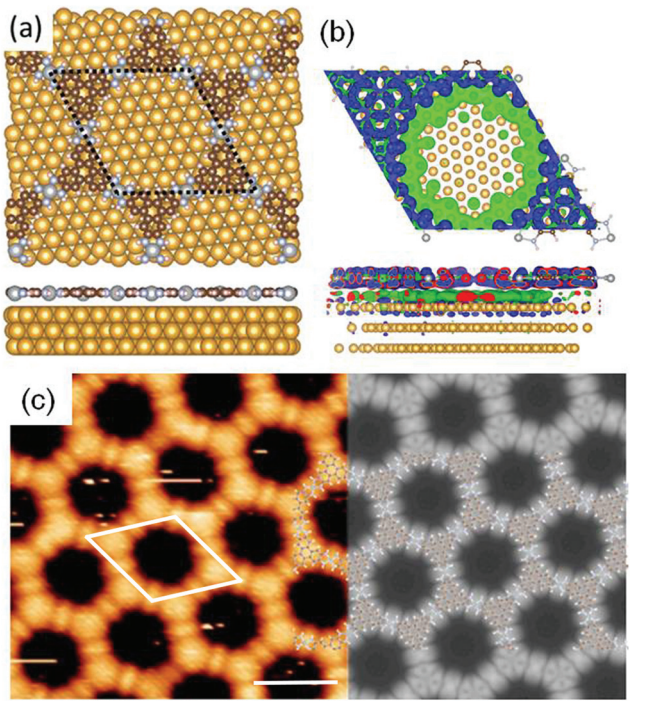

Fig. 2 (a) DFT optimized structure of the $Ni_3(HITP)_2$ single layer adsorbed on a Au(111)-$\sqrt{57} \times \sqrt{57}$ substrate. (b) Top and side views of charge transfer at an isosurface level of 2.87×10^{-4} e a^{-3} (a stands for Bohr radius). Green (blue) color represents charge accumulation (depletion), respectively. (c) Experimental (left) and simulated (right) STM images. Scale bar: 2 nm.

We further analyzed the charge transfer between the single-layer $Ni_3(HITP)_2$ and the Au(111) substrate. Fig. 2b shows the top and side views of charge redistribution at an isosurface level of 2.87×10^{-4} e a^{-3}. Here, we calculated the charge densities of three different systems, namely $Ni_3(HITP)_2$ on Au(111) ($\rho_{Ni\text{-}HITP/Au}(r)$), Au(111) substrate ($\rho_{Au}(r)$), and free-standing $Ni_3(HITP)_2$ ($\rho_{Ni\text{-}HITP}(r)$). We plot the charge redistribution following the equation, $\rho(r) = \rho_{Ni\text{-}HITP/Au}(r) - \rho_{Au}(r) - \rho_{Ni\text{-}HITP}(r)$. The top view in Fig. 2b (the green and blue colors represent charge accumulation and depletion, respectively) shows that the $Ni_3(HITP)_2$ layer transfers charge to the Au(111) substrate. The side view clearly visualizes charge depletion around the organic layer and charge accumulation near the Au surface. Overall, the $Ni_3(HITP)_2$ network is p doped when it is placed on the Au substrate. The charge transfer per unit cell is 0.82*e* (detailed analysis in the ESI†).

The electronic band structures of the $Ni_3(HITP)_2$ layer adsorbed on Au(111) are shown in Fig. 3. Black solid circles represent the contribution (>60%) of the $Ni_3(HITP)_2$ layer and they are mainly contributed from the p_z-orbital of the $Ni_3(HITP)_2$ layer. The grey lines denote the band structure of

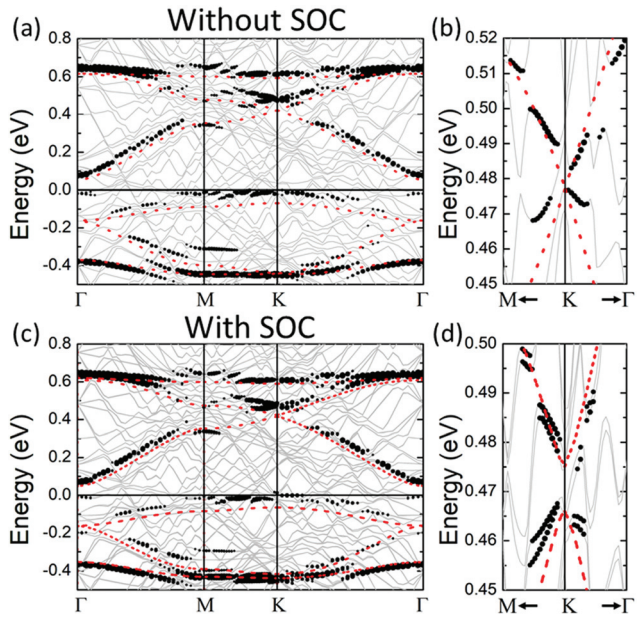

Fig. 3 DFT-calculated band structures of the $Ni_3(HITP)_2$ layer adsorbed on a Au(111)-$\sqrt{57} \times \sqrt{57}$ substrate without (a) and (b) with SOC. The black solid circles indicate the contribution (more than 60%) of the $Ni_3(HITP)_2$ network. The red dotted lines are the bands of a free-standing $Ni_3(HITP)_2$ network. (c) and (d) Zoom-in band structures of (a) and (b) near the *K* point. The bands of the free-standing $Ni_3(HITP)_2$ structure are up-shifted by 51 meV for comparison.

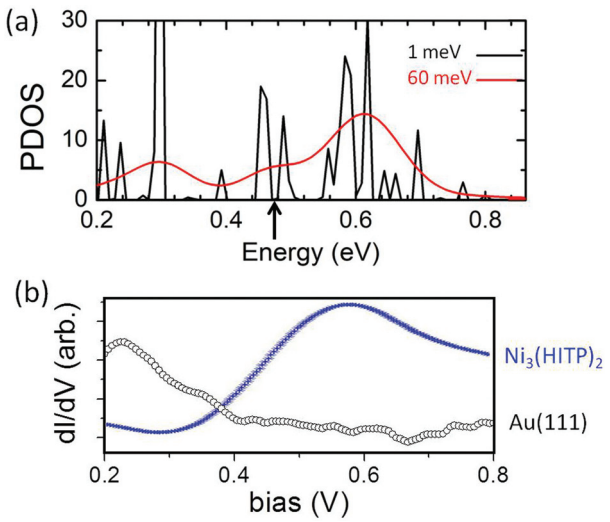

Fig. 4 (a) DFT-calculated projected density of states (PDOS) of the $Ni_3(HITP)_2$ monolayer (black: 1 meV smearing; red: 60 meV smearing). (b) Differential tunneling spectrum acquired at the $Ni_3(HITP)_2$ network (blue) and Au(111) surface (open dots).

the Au(111) substrate and most of the contribution comes from the s- and d-orbitals. The red dotted lines represent the band structure of a free-standing $Ni_3(HITP)_2$ structure. The highly dispersive band structures confirm the strong conjugation of the $Ni_3(HITP)_2$ structure. By comparison of the black and red dotted bands, one can see that the intrinsic band structure features of the free-standing $Ni_3(HITP)_2$ are largely retained in the surface-adsorbed single layer. The effective mass of the surface-adsorbed and the free-standing $Ni_3(HITP)_2$ layers for the electrons (holes) is 0.011 (0.018) and 0.008 (0.007) at the *K* point, respectively.

Furthermore, we find that a band gap is opened after including spin–orbit coupling (SOC) interactions. Fig. 3b and d show the zoom-in band structures around the *K* point, in which the bands of the free-standing $Ni_3(HITP)_2$ monolayer are also plotted (red dotted lines) and up shifted by 51 meV for comparison. With inclusion of SOC effects in the DFT calculations, a non-trivial gap of 8 meV is opened at the *K* point in the free-standing $Ni_3(HITP)_2$ monolayer. This value is almost the same as that of the free-standing system reported by Zhao *et al.*[12] This gap is maintained at the *K* points in the single-layer $Ni_3(HITP)_2$ adsorbed on the Au substrate, see the black dotted lines in Fig. 3d. Thus we argue that adsorption on Au (111) does not screen out the non-trivial topological effects of the $Ni_3(HITP)_2$ layer.

The DFT-calculated density of states projected to the $Ni_3(HITP)_2$ layer is plotted in Fig. 4a. When the PDOS is broadened by 1 meV (black curve), the topological gap around 0.47 eV renders a window featuring zero DOS as marked by the arrow. When the PDOS is broadened at 60 meV (red curve), the zero-DOS gap is not observable. The dispersive bands contribute a shoulder and a broad peak between 0.4 and 0.8 V. Experimentally, we used scanning tunneling spectroscopy to probe the electronic states of the $Ni_3(HITP)_2$ layer. The energy resolution of our tunneling spectroscopy measurements is 30 meV. The blue curve shown in Fig. 4b is the average of more than 100 differential tunneling (dI/dV) spectra acquired over a $Ni_3(HITP)_2$ network domain. It features a broad peak centered at 0.6 V, which is only present at the $Ni_3(HITP)_2$ network domains but not at the Au(111) surface (open dots). We assign this peak to the PDOS of the $Ni_3(HITP)_2$ layer around 0.6 eV in Fig. 4a. Due to the limited energy resolution, the non-trivial topological gap is not observed experimentally. It is worth noting that the domain size is about 40 nm across, corresponding to about 400 unit cells, in which the quantum size effect is negligible.[33]

Conclusions

In conclusion, we demonstrate that single-layer two-dimensional $Ni_3(HITP)_2$ can be synthesized on a Au(111) substrate. The Au substrate does not distort the geometric or electronic structure of the $Ni_3(HITP)_2$ structure. The strong conjugation of the $Ni_3(HITP)_2$ structure is manifested by highly dispersive bands as confirmed by DFT calculation and tunneling spectroscopy measurements. Particularly, a gap is opened when the SOC effect is switched on, implying that the quantum spin Hall phase of the free-standing layer is preserved in the surface-adsorbed single layer. To conduct quantum transport measurements and to explore the functionality of this system,

future work of growing or transferring the single layer to an insulating substrate is highly desirable.

Author contribution

Z. G., J. L. and R. Z. performed sample preparation and STM experiments, C.-H. H., F.-C. C., B. X., H. X. and L. H. performed DFT calculations, Q. J. and P. N. L. synthesized the HATP molecule, and N. L. designed and supervised the project and wrote the manuscript.

Conflicts of interest

There are no conflicts to declare.

Acknowledgements

The authors acknowledge the financial support from Hong Kong RGC16303514. C. H. and L. H. acknowledge the support by the NSFC under Grant No. 11704176 and 11774142, and the Shenzhen Peacock Plan Team under Grant No. KQTD2016022619565991. FCC acknowledges the support from the National Center for Theoretical Sciences and the Ministry of Science and Technology of Taiwan under Grant No. MOST 107-2628-M-110-001-MY3.

References

1 O. M. Yaghi, M. O'keeffe, N. W. Ockwig, H. K. Chae, M. Eddaoudi and J. Kim, *Nature*, 2003, **423**, 705.
2 S. Kitagawa, R. Kitaura and S. I. Noro, *Angew. Chem., Int. Ed.*, 2004, **43**, 2334.
3 R. Sakamoto, K. Takada, T. Pal, H. Maeda, T. Kambe and H. Nishihara, *Chem. Commun.*, 2017, **53**, 5781.
4 H. Maeda, R. Sakamoto and H. Nishihara, *Langmuir*, 2016, **32**, 2527.
5 F. Liu and J. Wu, *Natl. Sci. Rev.*, 2013, **1**, 32.
6 Z. F. Wang, Z. Liu and F. Liu, *Nat. Commun.*, 2013, **4**, 1471.
7 A. Bansil, H. Lin and T. Das, *Rev. Mod. Phys.*, 2016, **88**, 021004.
8 Z. F. Wang, Z. Liu and F. Liu, *Phys. Rev. Lett.*, 2013, **110**, 196801.
9 M. G. Yamada, T. Soejima, N. Tsuji, D. Hirai, M. Dincă and H. Aoki, *Phys. Rev. B: Condens. Matter Mater. Phys.*, 2016, **94**, 081102.
10 L. Dong, Y. Kim, D. Er, A. M. Rappe and V. B. Shenoy, *Phys. Rev. Lett.*, 2016, **116**, 096601.
11 X. Zhang, Z. Wang, M. Zhao and F. Liu, *Phys. Rev. B: Condens. Matter Mater. Phys.*, 2016, **93**, 165401.
12 B. Zhao, J. Zhang, W. Feng, Y. Yao and Z. Yang, *Phys. Rev. B: Condens. Matter Mater. Phys.*, 2014, **90**, 201403.
13 Z. Wang, N. Su and F. Liu, *Nano Lett.*, 2013, **13**, 2842.
14 O. J. Silveira, É. N. Lima and H. Chacham, *J. Phys.: Condens. Matter*, 2017, **29**, 09LT01.
15 Y. Wang, Y. Liu and B. Wang, *Sci. Rep.*, 2017, **7**, 41644.
16 L. Zhang, Z. Wang, B. Huang, B. Cui, Z. Wang, S. Du, H.-J. Gao and F. Liu, *Nano Lett.*, 2016, **16**, 2072.
17 Y. Wang, W. Ji, C. Zhang, P. Li, P. Wang, B. Kong, S. Li, S. Yan and K. Liang, *Appl. Phys. Lett.*, 2017, **110**, 233107.
18 O. J. Silveira, S. S. Alexandre and H. Chacham, *J. Phys. Chem. C*, 2016, **120**, 19796.
19 J. Cui and Z. Xu, *Chem. Commun.*, 2014, **50**, 3986.
20 R. Dong, M. Pfeffermann, H. Liang, Z. Zheng, X. Zhu, J. Zhang and X. Feng, *Angew. Chem., Int. Ed.*, 2015, **54**, 12058.
21 M. G. Campbell, D. Sheberla, S. F. Liu, T. M. Swager and M. Dincă, *Angew. Chem., Int. Ed.*, 2015, **54**, 4349.
22 D. Sheberla, L. Sun, M. A. Blood-Forsythe, S. L. Er, C. R. Wade, C. K. Brozek, A. N. Aspuru-Guzik and M. Dincă, *J. Am. Chem. Soc.*, 2014, **136**, 8859.
23 T. Kambe, R. Sakamoto, K. Hoshiko, K. Takada, M. Miyachi, J.-H. Ryu, S. Sasaki, J. Kim, K. Nakazato and M. Takata, *J. Am. Chem. Soc.*, 2013, **135**, 2462.
24 T. Kambe, R. Sakamoto, T. Kusamoto, T. Pal, N. Fukui, K. Hoshiko, T. Shimojima, Z. Wang, T. Hirahara and K. Ishizaka, *J. Am. Chem. Soc.*, 2014, **136**, 14357.
25 T. Pal, T. Kambe, T. Kusamoto, M. L. Foo, R. Matsuoka, R. Sakamoto and H. Nishihara, *ChemPlusChem*, 2015, **80**, 1255.
26 A. J. Clough, J. W. Yoo, M. H. Mecklenburg and S. C. Marinescu, *J. Am. Chem. Soc.*, 2014, **137**, 118.
27 X. Huang, P. Sheng, Z. Tu, F. Zhang, J. Wang, H. Geng, Y. Zou, C. Di, Y. Yi and Y. Sun, *Nat. Commun.*, 2015, **6**, 7408.
28 A. J. Clough, J. M. Skelton, C. A. Downes, A. A. De La Rosa, J. W. Yoo, A. Walsh, B. C. Melot and S. C. Marinescu, *J. Am. Chem. Soc.*, 2017, **139**, 10863.
29 N. Lahiri, N. Lotfizadeh, R. Tsuchikawa, V. V. Deshpande and J. Louie, *J. Am. Chem. Soc.*, 2016, **139**, 19.
30 G. Pawin, K. L. Wong, D. Kim, D. Sun, L. Bartels, S. Hong, T. S. Rahman, R. Carp and M. Marsella, *Angew. Chem., Int. Ed.*, 2008, **47**, 8442.
31 M. G. Campbell, S. F. Liu, T. M. Swager and M. Dincă, *J. Am. Chem. Soc.*, 2015, **137**, 13780.
32 L. Dong, Z. A. Gao and N. Lin, *Prog. Surf. Sci.*, 2016, **91**, 101.
33 R. Gutzler and D. F. Perepichka, *J. Am. Chem. Soc.*, 2013, **135**, 16585.